Substitutional nitrogen incorporation through rf glow discharge treatment and subsequent oxygen uptake on vertically aligned carbon nanotubes

Gamal Abbas,[1] Pagona Papakonstantinou,[1,*] Ganjigunte R. S. Iyer,[1] Ian W. Kirkman,[2] and Li C. Chen[3]
[1]*School of Electrical and Mechanical Engineering, University of Ulster at Jordanstown, Newtownabbey, County Antrim, BT37 0QB Northern Ireland, United Kingdom*
[2]*SERC, Daresbury Laboratory, CCLRC, Warrington WA4 4AD, Cheshire, England*
[3]*Center for Condensed Matter Sciences, National Taiwan University, Taipei 106, Taiwan*
(Received 19 February 2007; revised manuscript received 16 April 2007; published 21 May 2007)

By employing polarization- and temperature-dependent near-edge x-ray-absorption fine structure (NEXAFS) studies, we show that vertically aligned carbon nanotubes when subjected to low-pressure radio-frequency (rf) glow discharge can easily be doped with nitrogen atoms at predominantly graphitelike substitutional sites and at the same time preserve their vertical alignment in contrast to commonly used wet chemical functionalization methods. The O *K* edge NEXAFS spectra and angle-dependent x-ray phoelectron spectroscopy measurements established the presence of a significant amount of oxygen containing functional groups localized at the outer part of the walls. The amount of oxygen adsorbed on the carbon nanotubes is dependent on the introduction of nitrogen sites and exposed edge plane defects generated by plasma N treatment. Thermal gravimetric analysis measurements revealed a lower decomposition temperature for the plasma treated carbon nanotubes, which has its origin in the presence of a large fraction of active sites induced by rf glow discharge plasma treatment that accelerates the oxidation rate of N-doped carbon nanotubes. Our results indicate that rf low-pressure glow-discharge-mediated doping of nanotubes is a promising route to control the electronic structure of nanotubes and their reactivity due to introduction of active site defects.

DOI: 10.1103/PhysRevB.75.195429 PACS number(s): 61.46.Fg

INTRODUCTION

Chemical doping of sp^2 hybridized carbon systems such as carbon nanotubes (CNTs), fullerenes, and peapods is a possible route toward controllable modification of their electrical, optical, structural, mechanical, and physicochemical properties. Doping may be implemented by intercalating foreign atoms into the open space in the carbon network or by substituting the host atoms with impurities. For example, the intercalation of alkali metals into single-wall carbon nanotube (SWCNT) bundles has been shown to increase the conductivity.[1,2] The substitution of carbon atoms by nitrogen dopants has modified the structural properties of carbon nanotubes, giving them characteristic bamboo shaped structures[3] with improved field emission[4,5] and gas sensing characteristics. Their compartmentalized shapes can be explained in terms of pyridine-type nitrogen atoms (N atoms bonded to two carbon atoms, which are responsible for introducing corrugation within the system).

Nitrogen is a natural choice of dopant for carbon nanotubes because of its atomic radius similar to C. It also contains one electron more compared to C; therefore, the electronic structure contains donors responsible for generating *n*-type conductor.[6] The surface electronic structure of N-doped multiwall carbon nanotubes (MWCNTs) has been investigated using scanning tunneling spectroscopy, which revealed that the doped tubes have semimetallic properties and exhibit strong electron donor states near the Fermi level.[7] Moreover, the temperature-dependent thermoelectric power of N-doped carbon nanotube mats has been measured, showing that such dopant can be used to modify the majority-carrier conductivity.[8]

Nonmetallic impurities such as N, B, H, and O in π-conjugated carbon systems can, in principle, affect the magnetic properties of the material. The origin of this magnetism is still being debated. According to some recent reports, the defect induced magnetism appears to be one of the most probable scenarios for the origin of the observed carbon magnetism.[9,10] Structural defects, in particular, vacancy related defects, give rise to the development of magnetic ordering. Strong evidence supporting this scenario comes from recent experiments which demonstrate the development of induced magnetism in proton irradiated,[11] originally nonmagnetic graphite samples and in nanosized diamond particles irradiated by ^{15}N.[12] According to a recent theoretical investigation by Ma *et al.*, N adatoms on the surfaces of graphite and CNTs have localized magnetic moment.[13] Also, the substitutional N impurities enhance the magnetism of C adatoms by acting as attractors for mobile C, forming magnetic defect complexes.

Knowing the details of the interaction of N impurities with CNTs is very important for understanding and optimizing the nanotube doping process. Several growth methods based on arc discharge, chemical-vapor deposition, or substitutional reactions at high temperature are used nowadays to produce nitrogen-doped CNTs. Controlling the position of the nitrogen in the graphitic network (i.e., substitutional, pyridinic, gaseous nitrogen intercalated between graphite layers, nitrogen located in nonplanar sp^3 sites, chemisorbed) is important for understanding and optimizing the properties of nanotubes. In all directly grown CN_x nanotubes, the local environment of N within the carbon network mainly consists of N—C structures arranged in a pyridinelike configuration, which explains the metallic structure observed in these nanostructures.[8] Although there are many reports on the nitrogen doping of MWCNTs during growth,[14–16] or introduction of nitrogen bearing groups on nanotubes through chemi-

cal solution routes,[17–19] the postdeposition plasma nitrogenation of preformed CNTs is less explored. Only a handful of experiments have been done thus far with very limited information on the local atomic environment.[20,21] Most of these studies have used x-ray photoelectron spectroscopy (XPS), Raman spectroscopy, and Fourier transform infrared spectroscopy to probe the bonding configurations of functionalized nanotubes. Here, we show that due to its local character,[22–24] near-edge x-ray-absorption fine structure (NEXAFS) is a powerful technique for assessing the complex bonding configurations of the C and N atoms and their orientation.

Recently, we employed temperature-dependent NEXAFS spectroscopy to evaluate the local electronic structure of MWCNTs treated by atmospheric pressure filamentary dielectric barrier discharge (FDBD) plasma with ammonia as a carrier gas.[25] These nanotubes were in powder form, entangled, and were preprocessed in acids prior to FDBD functionalization. In the FD configuration, the plasma can be characterized as multiple tiny (0.1 mm in diameter) short-lived (10 ns) current filaments, called microdischarges.[26,27] This inherent filamentary character leads to accumulative thermal instability (i.e., arcing) and hence to nonuniform treatment by causing localized damage on the treated surfaces, which limits the applicability of the technique.[26,27] Hence, despite that DBD plasmas offer an economic route for technological application, they still lack the spatial homogeneity and stability of low-pressure plasmas. We were able to incorporate only 5 at. % N without obvious change in the oxygen content of CNTs. We showed that most of these N atoms were adsorbed to the CNT surface in the form of N-oxidic (NO) bonds without any significant change in the tabular structure of the nanotubes.[25]

Here, we wish to report that low-pressure radio-frequency (rf) glow discharge is an efficient and clean approach to dope carbon nanotubes with nitrogen atoms at predominantly substitutional sites and at the same time preserve their vertical alignment in contrast to commonly used wet chemical functionalization methods. In addition, we uncover that the amount of oxygen adsorbed on the carbon nanotubes is dependent on the introduction of nitrogen sites and exposed edge plane defects generated by plasma N treatment. These findings demonstrate that rf low-pressure glow discharge can be used as a route for implementing nanotubes in gas sensor applications.

EXPERIMENT

The pristine CNTs were grown by microwave chemical-vapor deposition on (100) silicon substrate using an 8-nm-thick Fe layer as a catalyst. Prior to CNT growth, hydrogen-plasma treatment (2 kW, 10 min) was employed for generating Fe catalyst nanoparticles.[28] For the growth process, the reactive gas mixture was $CH_4/H_2/N_2$ with fixed flow rates of 20/80/80 SCCM (SCCM denotes cubic centimeters per minute at STP). The applied microwave power during the growth of CNTs was 2 kW and the deposition time was kept at 10 min. The postdeposition N-doping process was carried out in a radio-frequency plasma-enhanced chemical-vapor deposition (PECVD) chamber using pure nitrogen gas at low pressure (2×10^{-6} Torr) and plasma powers of 100 and 200 W.

The measurements of NEXAFS were conducted at Station 1.1 of the Synchrotron Radiation Facility, SRS, at Daresbury Laboratory, and at Materials Science beamline of the ELETTRA synchrotron light source in Italy. The spectra at the C, N, and O *K* edges were recorded in surface sensitive total electron yield (TEY) mode. The monochromator energy scale was calibrated using the carbon *k* edge π^* of graphite, located at 285.35 eV. To eliminate the effect of incident beam intensity fluctuations and monochromator absorption features, the TEY signals were normalized using the incident beam intensity obtained from the photoemission yield of a clean Au grid, recorded simultaneously. The spectra have been processed through standard pre- and postedge normalization routines.[29] The preedge was subtracted to zero followed by postedge-jump normalization performed by dividing the preedge-jump normalized spectra by the edge jump intensity obtained far above the *K* edge, beyond 330 eV. This results in an edge jump of unity. Thus, changes in spectral intensity observed arise from anisotropy in the system and are independent of total carbon content. The jump of the C and N *K* edges at the ionization potential was fitted by an error function multiplied by an exponential decay function described by the following equation:[30]

$$I_{step} = H\left\{0.5 + 0.5\,\mathrm{erf}\left[\frac{(E-P)}{W/C}\right]\right\} \times \exp\{-[d(E-P-W)]\}, \quad E > P + W,$$

where H is the height of the function immediately above the step, E is the independent variable energy, P the position of the inflection point of the step, W is the full width at half maximum of the step, d is the exponential decay coefficient, and C is the constant defined by $c=2\sqrt{\ln 4}$. After subtracting the respective ionization jumps at both C *K* and N *K* edges, the resulting spectra were fitted using Gaussian peaks. Raman spectra were collected, employing a Labram 300 micro-Raman system using 632.8 nm excitation wavelength (He—Ne laser). The laser power impinging on the sample was kept constant at 3.5 mW with a 100× objective. Nine measurements were acquired at different locations on each sample and the average values were calculated for the peak positions and relative intensities. The Raman spectra were base line corrected using linear function and both *D* and *G* bands were fitted using a Lorentzian function. An AXIS ULTRA (Kratos) XPS spectrometer was used for the evaluation of C, N, and O contents in the CNT samples. The TGA was done with Pyris 1 TGA analyzer (Perkin Elmer). The tests were performed under flowing nitrogen atmosphere at a temperature range of 90–800 °C with a step of 25 °C/min.

RESULTS AND DISCUSSION

In order to fully understand the polarization trends for CNT samples, we initially studied the angular dependence of the C *K* edge NEXAFS of the highly ordered pyrolytic graphite (HOPG). The absorption spectra were recorded with

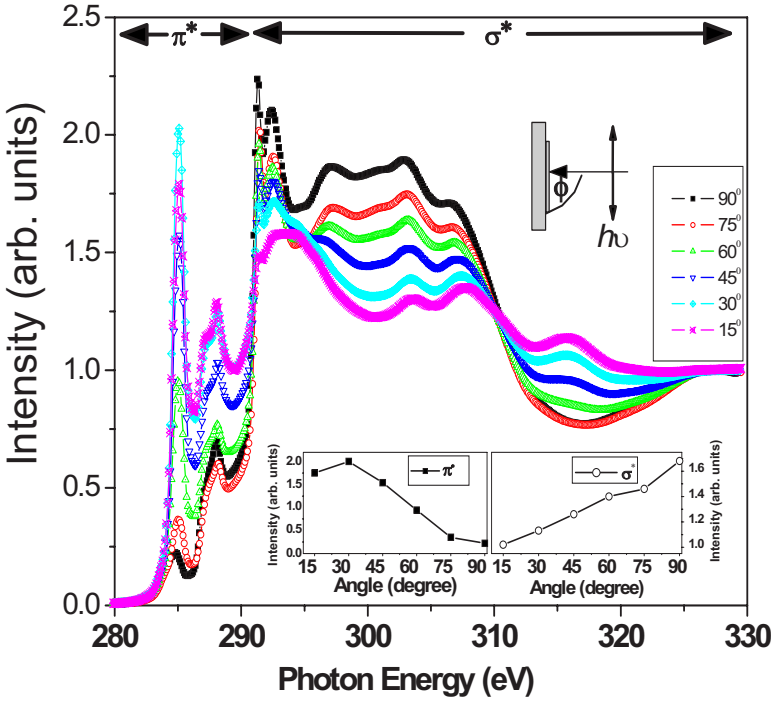

FIG. 1. (Color online) The polarization-dependent normalized C *K* edge NEXAFS spectra of highly oriented pyrolytic graphite (HOPG) sample. The upper inset shows a schematic of the incidence angle (ϕ). The lower insets show the intensity evolution of π^* and σ^* resonances at different angles.

the sample at different angles. The angle was measured between the pointing vector of the incident x-ray beam and the sample's surface (see the inset of Fig. 1). As shown in Fig. 1, the spectra exhibit a sharp π^* resonance near 285 eV and broad σ^* resonances in the region from 290 to 315 eV. In addition, there are two small peaks in the 287–290 eV region that are assigned to oxygenated surface functionalities[31] due to exposure to laboratory atmosphere.

In graphite, the six-member rings of carbon atoms all lie in planes (basal planes) parallel to the surface of the crystal and perpendicular to the crystallographic *c* axis. The π^* orbitals are aligned normal to the basal planes, whereas the σ^* orbitals are localized along the surface and normal to the crystallographic *c* axis. The maximum projection of the electric-field vector of the incident x-ray beam, **E**, onto a specific orbital, either π^* or σ^*, will result in maximum peak intensity. When the polarization vector **E** is parallel to the basal plane, only excitations to σ^* states are possible. Excitations to π^* states become more likely the more perpendicular to the basal plane the vector **E** is. This explains both trends of π^* and σ^* resonances with varying incident angle, as shown in the insets of Fig. 1. At a glancing incidence (15°), the π^* resonance shows maxima due to the large projection of **E** along the direction of π^* orbitals. Since the σ^* orbitals are orthogonal to the π^* orbitals, the σ^* bound exciton at ~292 eV exhibits the opposite trend, showing a minimal intensity. On the other hand, at normal incidence (90°), **E** is at 0° to the basal planes and perpendicular to the *c* axis and thus has no component along the π^* direction. This configuration results in a minimal intensity of the π^* resonance and a maximal intensity of the σ^* resonances.

Figures 2(a) and 2(b) show the angle-dependent C *K* edge NEXAFS spectra of pristine and N-doped CNT samples, respectively. The overall features of the electronic states of carbon atoms in the nanotubes are very similar to those of graphite. However, both CNT samples show a pronounced opposite angular dependence trend from that of the HOPG sample. Thus, the intensities of the π^* resonances are highest at normal incidence (90°) and lowest at glancing incidence (15°). These data point that the CNTs are oriented in a way that the hexagonal sheets are vertical to the silicon substrate (i.e., CNTs are grown vertically oriented to the silicon substrate). To quantify the degree of alignment in the CNTs and to evaluate the effect of plasma treatment on their alignment, we define an orientation parameter[32] (OP) as

$$\mathrm{OP} \equiv \frac{I_\perp - I_\parallel}{I_\perp + I_\parallel},$$

where $I_\perp$ is the π^* intensity at normal incidence (θ=90°) and $I_\parallel$ is the π^* intensity at grazing incidence (θ=0°). The value of $I_\parallel$ at 0° was obtained from a linear extrapolation of the $\sin^2\theta$ fit line for each of the samples to zero in Fig. 2(c). The OPs for HOPG graphite, pristine CNT, doped CN_x(200 W), and doped CN_x(100 W) samples were found to be −0.8, 0.5, 0.4, and 0.49, respectively. From the definition of the order parameters described above, one should note that values close to 1 indicate higher order. The negative sign indicates that the π^* resonance decreases in intensity with the increase of θ. One can conclude that the surfaces of the three CNT sample arrays (upper 10 nm) are relatively ordered in comparison to well oriented sheets of HOPG (see Fig. 3). Most importantly, the data demonstrate that the rf glow discharge plasma preserved the alignment of the pristine CNT in contrast to commonly wet chemical functionalization methods. This is a very important result as the successful use of CNTs in many applications, such as sensors, probe tips, and field-effect emitters, requires control of the growth direction.

Figure 4(a) shows the normalized angle-dependent NEXAFS spectra at the N 1*s* edge for the N-plasma treated carbon nanotube (CN_x) sample at a power of 200 W. The inset

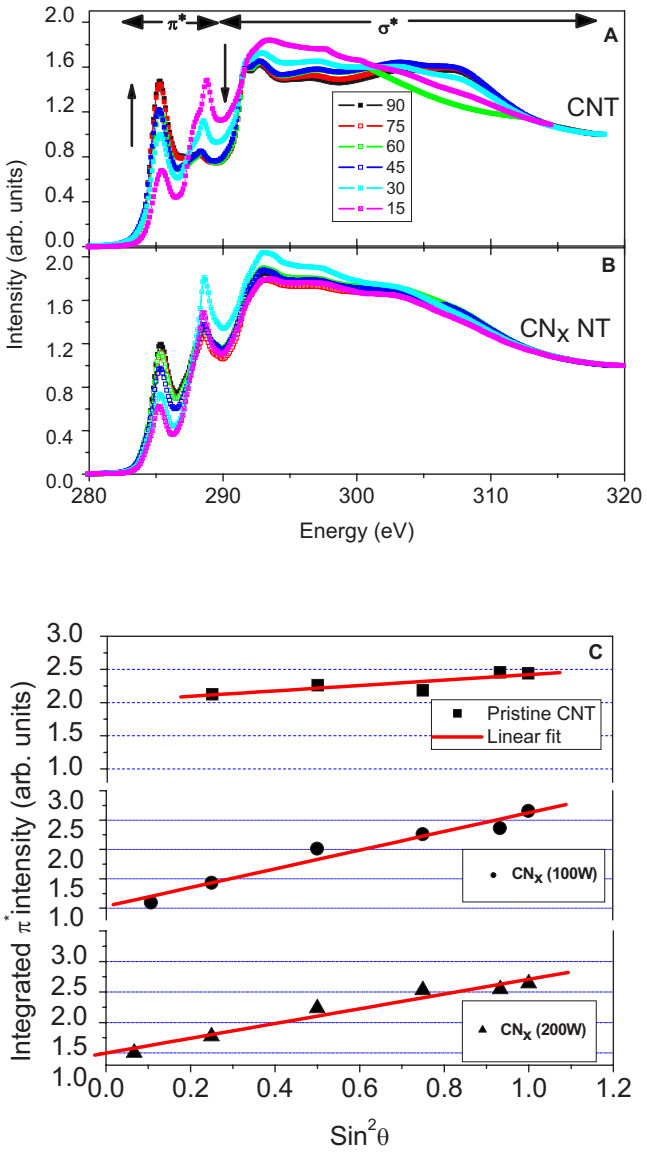

FIG. 2. (Color online) The angular dependence of the normalized NEXAFS spectra of (a) pristine and (b) N-doped CNT samples at the C *K* edge. (c) The pristine and N-doped CNT integrated intensity of π^* peaks fitted to $\sin^2\theta$.

shows a representative deconvolution where well resolved π^* resonances, N1, N2, and N3, dominate the N 1*s* spectra at energies of 398.3, 399.5, and 400.8 eV, respectively, and a broad resonance starting at ~405 eV represents the σ^* region. These π^* resonances indicate the existence of various C—N π^* bonds in the local structure. The N1, N2, and N3 resonances represent the nitrogen atoms' absorption in pyridinelike structure, cyanic structure, and substitutional graphitelike structure, respectively. The assignment of these peaks is in agreement with previous observations in different CN_x structures.[33,34] A polarization dependence of a N π^* resonance similar to that of the C π^* resonance, illustrated in Fig. 2, would indicate that the nitrogen atoms are in plane of graphite sheet. Figure 4(b) clearly shows that both N1 and N3 have similar trend; however, the intensity of N3 considerably changes with incidence angle. The N3 and N2 peaks show a graphitelike π^* CNT polarization dependence,

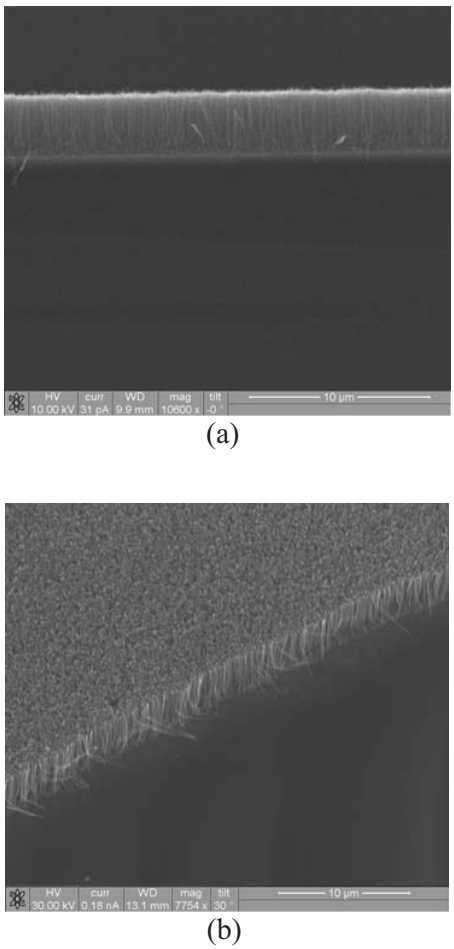

FIG. 3. SEM images of highly oriented (a) pristine CNT and (b) CN_x NT sample with different magnifications.

namely, the peaks are weak at grazing incidence and enhanced at normal incidence, while the peak N2 has opposite polarization dependence. The intense N3 peak indicates that a considerable amount of nitrogen atoms are substitutionally incorporated in the hexagonal graphitelike structure, i.e., N atoms replace C atoms in graphite rings and every nitrogen atom is bonded to three carbon atoms. On the other hand, since the cyanic structure and graphite basal plane join with only a single C—C bond, it is expected that this structure will have an upright standing orientation to graphite basal plane. This is in agreement with the opposite polarization dependence of N3 and N2 peaks, and therefore, the N2 is assigned to the cyanic structure.[31]

We have to emphasize that the local N bonding environment in the present study is clearly different from that of ammonia treated entangled MWCNT samples using the atmospheric plasma FDBD system.[25] In the latter samples, temperature-dependent NEXAFS studies confirmed that the NO functional groups dominated the N local structure (Fig. 2 in Ref. 25). These findings clearly demonstrate that the type of plasma source (DBD, rf glow discharge) and therefore the nature of impinging particles and the tubes' history all have major effects on the final chemical bonding and composition of the functionalized CNT.

Next, we carried out NEXAFS studies on thermally annealed CN_x nanotubes with a view of providing an insight on

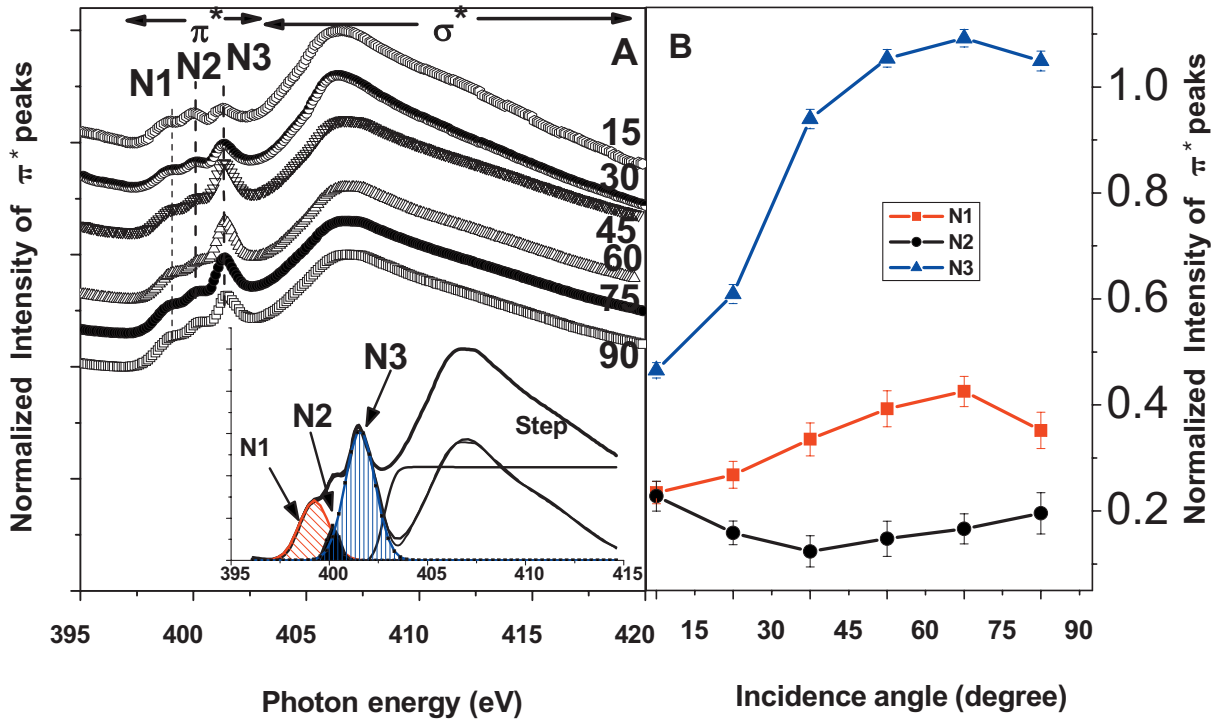

FIG. 4. (Color online) (a) The angle-dependent N *K* edge NEXAFS spectra of CN_x NT sample. The inset shows representative deconvolution of the NEXAFS spectrum. (b) The variation of π^* peak intensities at N *K* edge with incidence angle (ϕ).

the temperature evolution of the local electronic structure of the films and confirm our previous assignments. Figures 5(a)–5(c) shows the normalized N *K* edge NEXAFS spectra together with the corresponding convoluted peaks N1, N2, and N3 of *in situ* thermally annealed CN_x nanotubes, measured at normal incidence. One may note that the spectra are not exactly the same as those presented in Figs. 4. The signal-to-noise ratio in the current figure is lower in comparison to that of Fig. 4. The reason for this inconsistency is that the spectra in Fig. 5(a) were taken at a different station (i.e., ELETTRA synchrotron). Figure 5(d) provides the trends of the N peaks as a function of annealing temperature. One can observe a clear enhancement on peak N3 at the annealing temperature of 800 °C in comparison to N1 and N2. Studies on the thermal stability of carbon nitride (CN_x) film by Shimoyama *et al.*[33,34] showed that the graphitelike structures become dominant by annealing at 1100 °C. Therefore, the increase of the intensity of peak N3 at higher temperatures indicates the formation of substitutional graphitelike structure, which is consistent with our previous assignment. As the temperature increases, the nitrogen is driven out of the bonded matrix. This result is supported by the narrowing of the σ^* resonance at the N *K* edge, indicating a clear loss of C—N bonds.[25]

Figure 6 presents a comparison of the C *K* edge NEXAFS spectra of as-grown and nitrogen-doped CNT samples at θ values of (a) 90°, (b) 60°, and (c) 30°. The general features of the spectra appear to be similar, though their intensities are different. The following important features can be identified in the spectra of CN_x nanotubes: (i) the intensity of the C—C π^* resonance exhibits lower intensity and less broadening, (ii) the σ^* resonance is more intense and has lost its sharpness, and finally (iii) the intensity of the two peaks (the first appear as shoulder) in the 287–290 eV region becomes prominent. These two peaks were previously assigned, by Banerjee *et al.*, to π^*C═O and σ^*C—O transitions in ozonized[35] SWCNTs. In a later study, a similar diminution of π^* peak intensity with respect to the strength of the σ^* peak was observed as the SWCNTs were increasingly oxidized. These observations are consistent with the loss of the characteristic electronic transitions between the intrinsic van Hove singularities in functionalized nanotubes caused by the disruption of the π network upon sidewall functionalization.[36,37]

In the current study, both NEXAFS and XPS highlight the presence of significant oxygen containing functional groups in the CN_x NT sample. Figure 7 shows the angle-dependent O *K* edge normalized NEXAFS spectra of the CN_x NT. The spectra contain two main features: (i) one at 534 eV, which is assigned to a π^* (CO) resonance, and (ii) a broader asymmetric peak at 538 eV, associated with σ^* (CO) resonances.[31] Upon changing the incidence angle, the π^* and σ^* features show an opposite polarization dependence, which is expected from the normal orientation of π^* and σ^* orbitals. There are two possible routes for the oxygen uptake on CN_x. Firstly, it could happen *in situ* during the plasma treatment due to residual water or excess oxygen in the reactor chamber. Secondly, it could happen *ex situ* upon exposure of the samples to the laboratory's atmosphere. The latter could take place as a result of the plasma activation of adsorption sites (creation of defects). To further elucidate the origin of this oxygen uptake, we have performed Raman and angle-resolved XPS spectroscopic studies.

XPS measurements revealed a substantial increase on the atomic concentration of oxygen from 1.1 at. % for pristine

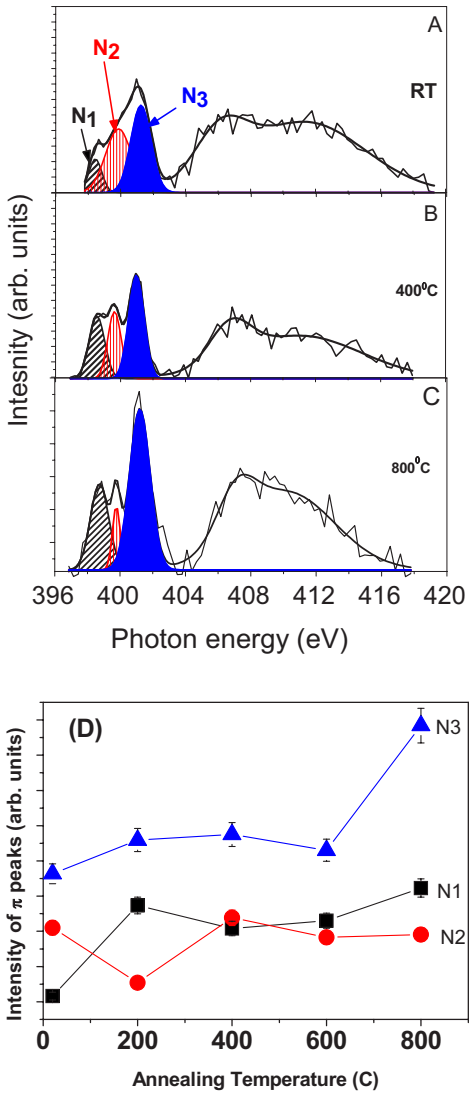

FIG. 5. (Color online) The deconvolution of N *K* edge spectra of CN_x NT sample, measured at normal incidence, as a function of annealing temperatures: (a) RT, (b) 400 °C, and (c) 800 °C. (d) The evolution of individual nitrogen π^* peaks with annealing temperatures.

CNTs to 13.9 at. % for nanotubes treated at a plasma bias of 100 W (see Table I and Fig. 8). It has been reported that N-doped MWCNTs and graphite treated in nitrogen atmosphere are chemically reactive due to the presence of pyridine defect sites with unpaired electrons.[4,5] Figures 8(b)–8(d) show the C, N, and O *K* edge XPS spectra of three CN_x NT samples treated at 0, 100, and 200 W, taken at normal (90°) incidence. Upon increasing the plasma power from 100 to 200 W although there is no appreciable variation on the nitrogen content (12.3 and 13.7 at. %), a significant enhancement on the oxygen content from 13.9 to 21.7 at. % respectively, is observed. On the other hand, angle-resolved XPS measurements presented in Table I show an even greater variation on the oxygen content at grazing incidence (15°). At grazing angle, the oxygen content of the same samples (100 and 200 W) increases from 19.6 to 40.9 at. %, respectively. Normal angle of incidence provides more information on the inner part of the wall because of the larger escape depth of the photoelectrons. Overall, at grazing angle the oxygen concentration is increasing compared to normal incidence, indicating a higher O concentration in the outer part of the wall.

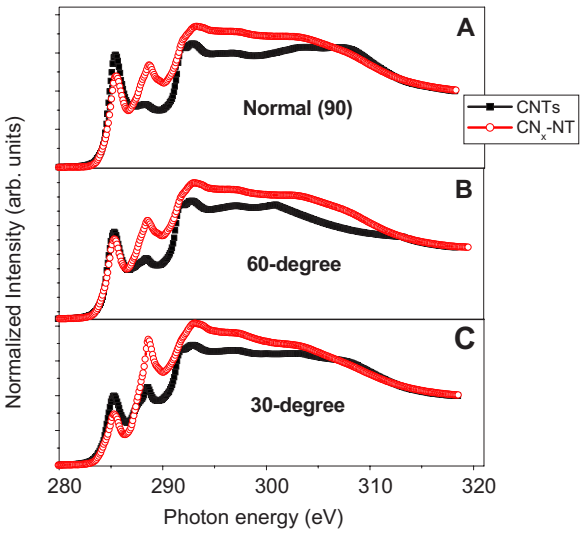

FIG. 6. (Color online) The C *K* edge normalized NEXAFS spectra of pristine CNT and CN_x NT samples measured at (a) normal (90°), (b) 60°, and (c) glancing (30°) angles.

The significant difference on oxygen concentration with the plasma power can be explained only by considering a larger number of defects generated at increased plasma power conditions (more energetic at 200 W). These findings are consistent with the notion that N_2 plasma treatment at 200 W creates nitrogen related defects as well as an increased amount of unsaturated carbon atoms at graphene edge sites; these sites are very active for subsequent oxygen adsorption. The presence of these defects on the outer wall(s), as indicated by shallow-depth XPS measurements, enhances the probability of attracting oxygen once the sample is exposed to the atmosphere. Additionally, our previous study on atmospheric DBD plasma functionalization[25]

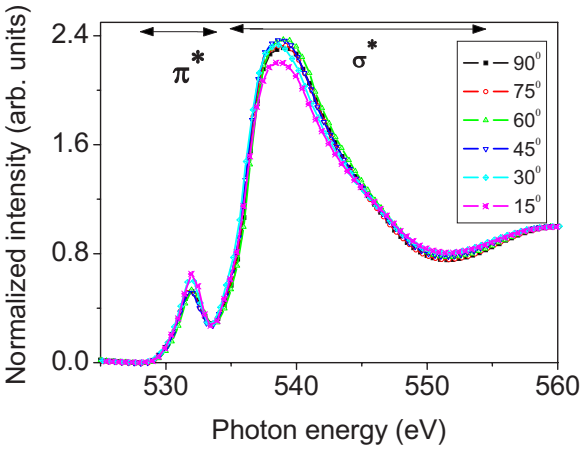

FIG. 7. (Color online) The O *K* edge normalized NEXAFS spectra of CN_x NT sample as a function of incidence angle (ϕ). One could notice that there is a slight angle dependence.

TABLE I. Variation of C, N, and O atomic % in pristine and N-plasma samples treated at different plasma powers and measured at varying depth using angle-dependent XPS technique.

	Concentration (at. %)					
	Pristine CNT		Plasma treated CNT at 100 W		Plasma treated CNT at 200 W	
XPS peak	90° (Normal)	15° (Grazing)	90° (Normal)	15° (Grazing)	90° (Normal)	15° (Grazing)
C 1*s*	96.16	95.54	73.82	69.99	64.62	48.18
N 1*s*	2.73	3.2	12.29	10.43	13.7	10.86
O 1*s*	1.11	1.26	13.89	19.58	21.69	40.96

did not show any obvious change in the oxygen content of CNTs. Therefore, residual water or/and excess oxygen do not seem to be the source for the significant oxygen uptake on the CN_x surface.

Figure 9 shows the micro-Raman spectra from pristine and nitrogenated MWCNTs samples using He—Ne laser (i.e., 633.5 nm excitation wavelength). The spectra of the as-deposited CNTs exhibited the well defined *G* band (graphitelike E_{2g} stretching vibration of sp^2 carbon bonds) and the disorder-induced band (or *D* band) at 1587 and 1352 cm^{-1}, respectively. The *D* band is present in all known forms of disordered sp^2 carbons and has been identified with C atom vacancy substitutional impurities, finite grain and particle effects, or any other symmetry-breaking phenomena.[36,37] The I_D/I_G ratio increases from 1.24 for the pristine sample to 1.4 for the plasma treated sample (see the inset of Fig. 1). Hence, there is a decline of the structural order due to the induced structural defects (for example, introduction of sp^3 covalent bonds) caused by the N-plasma treatment.

TGA was conducted to assess the thermal oxidation behavior of CNTs. Figure 10 shows typical TGA curves for CNTs treated with N plasma at different powers (i.e., 0, 100, and 200 W). The TGA curves show an initial gradual change in sample weight followed by an abrupt drop as the temperature increases. The maxima in first derivative plots, dW/dT, of the TGA curves are used to estimate burnoff temperatures of the CNTs in an inert gas (i.e., nitrogen). The weight loss derivatives, dW/dT, for all the samples exhibit a single peak as a function of *T*. The burnoff temperatures decreased from 696.5 ± 10 °C for the pristine sample to 575 ± 5 and 548 ± 10 °C for CN_x treated samples at 100 and 200 W, respectively.

At first glance, it seems that there is a contradiction on the evaluation of the thermal stability of CN_x nanotubes, obtained from TGA and *in situ* rapid thermal annealing NEXAFS study (Fig. 5). Temperature-dependent NEXAFS data revealed that the CN_x nanotubes were stable up the highest used temperature of 800 °C. This contradiction can be lifted by taking into account the different environment and time the measurements were conducted. In the NEXAFS study, an e-beam was used to heat the CN_x CNT/Si sample for 2 min under high vacuum (2.6×10^{-7} Torr), whereas the TGA analysis was a slow process, performed on CN_x nanotube powder of less than 1 mg under flowing nitrogen atmosphere with an annealing rate of 15 °C/min up to 900 °C.

Concerning the TGA oxidation behavior, Maldonado and Stevenson observed similar deterioration in the thermal sta-

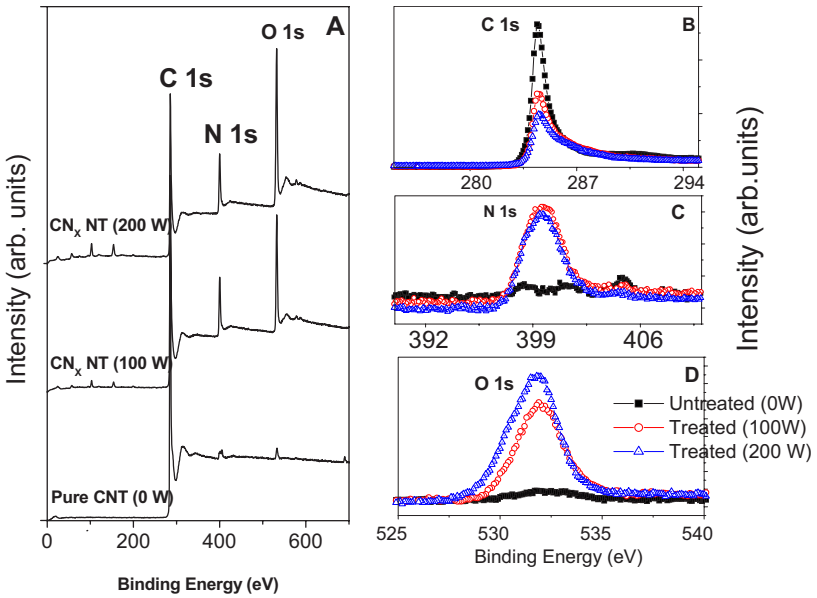

FIG. 8. (Color online) (a) XPS survey spectra, measured at normal incidence (90°), for identical CNT samples treated with nitrogen plasma (CN_x NT) at 0, 100, and 200 W. [(b)–(d)] XPS spectra of the same samples at C *K* edge, N *K* edge, and O *K* edge, respectively.

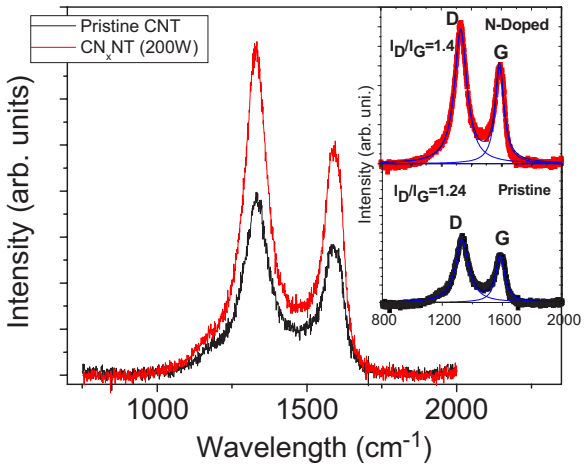

FIG. 9. (Color online) Variation in Raman spectra of a pristine CNT sample after N-plasma treatment at 200 W. The insets show representative fittings for both samples.

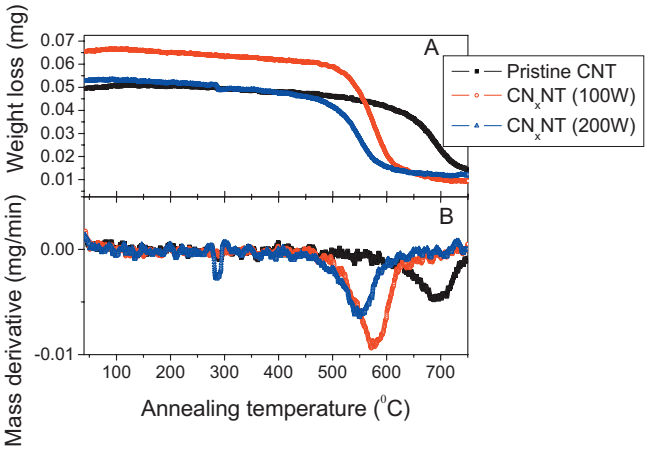

FIG. 10. (Color online) (a) Thermal gravimetric analysis (TGA) and (b) the derivative of the TGA curves for pristine and CN_x nanotubes treated at power values of 0, 100, and 200 W.

bility of carbon nanofibers (CNFs) caused by N-doping process.[38] They supported their claims by using transmission electron microscopy analysis to confirm the disordering and compartmentalization in the sidewalls of N-doped CNF. This nitrogen induced disordering has been confirmed by our NEXAFS spectroscopic data. The loss of the excitonic σ^* peak in Fig. 2(b) [observed in pristine CNT, Fig. 2(a)] indicates an occurrence of short-range disorder in these CN_x NT.[39] In the present study, since the CN_x NT samples treated at different powers (100 and 200 W) contain almost the same nitrogen concentration, one could assume that the high power plasma has induced a larger fraction of active sites, which accelerates the oxidation rate of the CN_x nanotubes.[40,41]

CONCLUSION

Angle- and temperature-dependent NEXAFS spectroscopy was employed to study the electronic and structural properties of highly oriented MWCNT treated with pure N plasma using low-pressure rf-PECVD route at room temperature. Interestingly, the N *K* edge spectra of CN_x nanotubes showed that majority of the N atoms were introduced as substitutional graphitic nitrogen with small percentages incorporated in a pyridinelike structure and cyanic structure. This is in contrast to studies on directly grown nanotubes in nitrogen atmosphere, where the majority of nitrogen atoms were introduced in pyridine sites. Angle-dependent NEXAFS studies confirmed that the vertical alignment of nanotubes is preserved after plasma treatment. This opens an avenue for functionalization, where the conservation of vertical alignment is important (e.g., nanoelectronic applications). The O *K* edge NEXAFS and XPS spectra revealed that the oxygen functionalities were substantially improved after N-plasma treatment. Low-pressure rf plasma treatment is an effective route on introducing nitrogen atoms on the hexagonal lattice; however, it leaves the surface with very high reactive sites capable of adsorbing oxygen. We envisage that rf glow discharge could be a route for implementing nanotubes, in gas sensor applications. TGA provided evidence that the plasma power was an important factor that affected the thermal stability of the CNTs by increasing the degree of their structure disorder and reactivity.

ACKNOWLEDGMENTS

The NEXAFS measurements were performed at the CCRLC facility at Daresbury, UK (Station 2.3) and ELETTRA synchrotron at Trieste, Italy (Station 6.1 L). The authors acknowledge the European Union under the DESYGN-IT project (STREP Project No. 505626-1) and the Royal Society (Taiwan-UK joint project).

*Author to whom correspondence should be addressed. Fax: +44 (0)28 90366863. Email address: p.papakonstantinou@ulster.ac.uk

[1] S. Lee, H. J. Kim, J. E. Fisher, A. Thess, and R. E. Smalley, Nature (London) **388**, 255 (1997).

[2] H.-S. Ahn, K.-R. Lee, and S. Han, Appl. Phys. Lett. **88**, 093122 (2006).

[3] R. C. Che, L. M. Peng, and M. S. Wang, Appl. Phys. Lett. **85**, 4753 (2004).

[4] J. W. Jang, C. E. Lee, S. C. Lyu, T. J. Lee, and C. J. Lee, Appl. Phys. Lett. **84**, 2877 (2004).

[5] M. Terrones, Int. Mater. Rev. **49**, 325 (2004).

[6] K. Xiao, Y. Q. Liu, P. A. Hu, G. Yu, Y. M. Sun, and D. B. Zhu, J. Am. Chem. Soc. **127**, 8614 (2005).

[7] R. Czerw, M. Terrones, J. C. Charlier, X. Blase, B. Foley, R. Kamalakaran, N. Grobert, H. Terrones, D. Tekleab, P. M. Ajayan, W. Blau, M. Ruhle, and D. L. Carroll, Nano Lett. **1**, 457

(2001).
[8] Y. M. Choi, D. S. Lee, R. Czerw, P. W. Chiu, N. Grobert, M. Terrones, M. Reyes-Reyes, H. Terrones, J. C. Charlier, P. M. Ajayan, S. Roth, D. L. Carroll, and Y. W. Park, Nano Lett. **3**, 839 (2003).
[9] A. N. Andriotis, R. M. Sheetz, and M. Menon, Phys. Rev. B **74**, 153403 (2006).
[10] P. O. Lehtinen, A. S. Foster, Yuchen Ma, A. V. Krasheninnikov, and R. M. Nieminen, Phys. Rev. Lett. **93**, 187202 (2004).
[11] P. Esquinazi, D. Spemann, R. Hohne, A. Setzer, K. H. Han, and T. Butz, Phys. Rev. Lett. **91**, 227201 (2003).
[12] S. Talapatra, P. G. Ganesan, T. Kim, R. Vajtai, M. Huang, M. Shima, G. Ramanath, D. Srivastava, S. C. Deevi, and P. M. Ajayan, Phys. Rev. Lett. **95**, 097201 (2005).
[13] Y. Ma, A. S. Foster, A. V. Krasheninnikov, and R. M. Nieminen, Phys. Rev. B **72**, 205416 (2005).
[14] J. Liu, S. Webster, and D. L. Carroll, Appl. Phys. Lett. **88**, 213119 (2006).
[15] S. Maldonado, S. Morin, and K. Stevenson, Carbon **44**, 1429 (2006).
[16] H. C. Choi, S. Y. Bae, J. Parka, K. Seo, C. Kim, B. Kimc, H. J. Song, and H.-J. Shin, Appl. Phys. Lett. **85**, 5742 (2004).
[17] C. A. Dyke and J. M. Tour, Chem.-Eur. J. **10**, 812 (2004).
[18] T. Ramanathan, F. T. Fisher, R. S. Ruoff, and L. C. Brinson, Chem. Mater. **17**, 1290 (2005).
[19] S. E. Baker, W. Cai, L. Tami, T. L. Lasseter, K. P. Weidkamp, and R. J. Hamers, Nano Lett. **2**, 1413 (2002).
[20] B. Khare, P. Wilhite, B. Tran, E. Teixeira, K. Fresquez, D. N. Mvondo, C. Bauschlicher, and M. Meyyappan, J. Phys. Chem. B **109**, 23466 (2005).
[21] B. N. Khare, P. Wilhite, R. C. Quinn, B. Chen, R. H. Schingler, B. Tran, H. Imanaka, C. R. So, C. W. Bauschlicher, and M. Meyyappan, J. Phys. Chem. B **108**, 8166 (2004).
[22] T. M. Minea, B. Bouchet-Fabre, S. Lazar, S. Point, and H. W. Zandbergen, J. Phys. Chem. B **110**, 15659 (2006).
[23] Y. F. Jia, Q. Zhu, and K. M. Thomas, Chem. Phys. Lett. **364**, 171 (2002).
[24] I. Jimenez, W. M. Tong, D. K. Shuh, B. C. Holloway, M. A. Kelly, P. Pianetta, L. J. Terminello, and F. J. Himpsel, Appl. Phys. Lett. **74**, 2620 (1999).
[25] S. S. Roy, P. Papakonstantinou, T. I. T. Okpalugo, and H. Murphy, J. Appl. Phys. **100**, 053703 (2006).
[26] C. Sarra-Bournet, S. Turgeon, D. Mantovani, and G. Laroche, J. Phys. D **39**, 3461 (2006).
[27] J. Ráhel' and D. M. Sherman, J. Phys. D **38**, 547 (2005).
[28] L. C. Chen, C. Y. Wen, C. H. Liang, W. K. Hong, K. J. Chen, H. C. Cheng, C. S. Shen, C. T. Wu, and K. H. Chen, Adv. Funct. Mater. **12**, 687 (2002).
[29] S. Banerjee, T. Hemraj-Benny, S. Sambasivan, D. A. Fischer, J. A. Misewich, and S. S. Wong, J. Phys. Chem. B **109**, 8489 (2005).
[30] D. A. Outka and J. Stohr, J. Chem. Phys. **88**, 3539 (1988); S. Bhattacharyya, M. Lqbbe, and F. Richter, J. Appl. Phys. **88**, 5043 (2000).
[31] A. Kuznetsova, I. Popova, J. T. Yates, M. J. Bronikowski, C. B. Huffman, J. Liu, R. E. Smalley, H. H. Hwu, and J. G. Chen, J. Am. Chem. Soc. **123**, 10699 (2001).
[32] T. Sakai, K. Ishikawa, H. Takezoe, N. Matsuie, Y. Yamamoto, H. Ishii, Y. Ouchi, H. Oji, and K. Seki, J. Phys. Chem. B **105**, 9191 (2001).
[33] I. Shimoyama, G. Wu, T. Sekiguchi, and Y. Baba, Phys. Rev. B **62**, R6053 (2000).
[34] I. Shimoyama, G. Wu, T. Sekiguchi, and Y. Baba, J. Electron Spectrosc. Relat. Phenom. **114–116**, 841 (2001).
[35] S. Banerjee, T. Hemraj-Benny, M. Balasubramanian, D. A. Fischer, J. A. Misewich, and S. S. Wong, Chem. Commun. (Cambridge) **2004**, 772.
[36] *Analytical Applications of Raman Spectroscopy*, edited by M. J. Pelletier (Blackwell Science, Oxford, 1999).
[37] M. J. Matthews, M. A. Pimenta, G. Dresselhaus, M. S. Dresselhaus, and M. Endo, Phys. Rev. B **59**, R6585 (1999).
[38] S. Maldonado and K. J. Stevenson, J. Phys. Chem. B **109**, 4707 (2005).
[39] M. Rao, P. C. Eklund, S. Bandow, A. Thess, and R. E. Smalley, Nature (London) **388**, 257 (1997).
[40] N. Laine, F. Vastola, and P. Walker, J. Phys. Chem. **67**, 2030 (1963).
[41] N. Welham and J. Williams, Carbon **36**, 1309 (1998).